Assessment of Off-Design Low-Boom Characteristics of a Low-Boom Supersonic Transport

Wu Li* and Karl Geiselhart†
NASA Langley Research Center, Hampton, Virginia 23681, USA

Most conceptual design methods for low-boom supersonic aircraft are developed for achieving an undertrack low-boom goal at the start of cruise. Although attempts have been made to design a supersonic aircraft achieving a low-boom goal for multiple azimuthal angles at the start of cruise, one unanswered question in inverse design optimization is how to define an achievable low-boom goal for multiple azimuthal angles. This paper proposes a new analysis method to assess off-design low-boom characteristics of a low-boom supersonic transport designed for an undertrack low-boom goal at the start of cruise. This method opens a potentially feasible path for conceptual design of a supersonic aircraft that has desired low-boom characteristics over the primary boom carpet for the entire cruise segment.

Nomenclature

A_e	=	any equivalent area including $A_{e,CFD}$ and $A_{e,r}$, ft^2
$A_e(\theta)$	=	equivalent area for azimuthal angle θ, ft^2
$A_{e,r}^{target}(\theta)$	=	selected Pareto point as the target for $A_{e,r}$ of a supersonic concept for azimuthal angle θ, ft^2
$A_{e,CFD}$	=	equivalent area defined using Mach angle cut method and computational fluid dynamics, ft^2
$A_{e,pareto}(\theta)$	=	Pareto optimal equivalent area target for a pair of cruise condition and azimuthal angle θ, ft^2
$A_{e,r}$	=	reversed equivalent area defined by using reverse propagation of off-body pressure, ft^2
$A_{e,r}(\theta)$	=	reversed equivalent area for azimuthal angle θ, ft^2
$\boldsymbol{d}$	=	vector of shape parameters for $A_e(\theta)$
dp/p	=	nondimensional overpressure $(p–p_\infty)/p_\infty$
$\boldsymbol{D}$, $\boldsymbol{D}_0$	=	vector of design variables that define a supersonic aircraft
l_e	=	effective length of supersonic configuration, which is the largest effective distance where Mach angle cut plane intersects the configuration, ft
p	=	longitudinal pressure distribution at off-body location, lb/ft^2
p_∞	=	ambient pressure, lb/ft^2
PLdB(A_e)	=	perceived level in decibels for ground signature of A_e
t	=	variable for a parametric Bezier curve
x_e	=	effective distance for A_e, ft
ϵ	=	acceptable error tolerance for inverse design of $A_{e,r}$, ft^2
θ	=	azimuthal angle for sonic boom propagation, deg
$\lVert\cdot\rVert$	=	2-norm of a function f on interval [0, l_e] defined by $\lVert f\rVert$, which equals $\left(\int_0^{l_e} \lvert f(t)\rvert^2\, dt \,/ l_e\right)^{\frac{1}{2}}$

I. Introduction

THE ban on overland supersonic flights is a key barrier for the development of commercial supersonic aircraft. To help lift this ban, NASA has been developing low-boom technologies that will enable a commercially successful supersonic transport to fly overland with a quiet sonic thump on the ground, instead of a loud sonic boom. The NASA N+3 low-boom goal [1] is that a commercial supersonic transport will only create sonic boom ground signatures with perceived levels in decibels (PLdB) [2] below 70, which is significantly lower than the sonic boom loudness values exceeding 100 PLdB for Concorde (see page 6 of Ref. [1]). The X-59, NASA's quiet supersonic experimental aircraft, has been designed using computational fluid dynamics (CFD) based low-boom shaping technologies to demonstrate

* Senior Research Engineer, Aeronautics Systems Analysis Branch
† Aerospace Engineer, Aeronautics Systems Analysis Branch

a sonic thump of about 75 PLdB on the ground [3,4]. Although low-boom shaping technologies have reasonably matured, a simultaneous achievement of design goals for aerodynamic efficiency and low-boom shaping of the outer mold line (OML) of a commercial supersonic transport is still extremely challenging. Our recent work using a multiobjective multidisciplinary optimization (MDO) method called the block coordinate optimization (BCO) method demonstrated success on that front in the conceptual design phase. The BCO method dissects a multiobjective low-boom MDO problem into several weakly coupled and solvable optimization subproblems. These optimization subproblems are solved successively and repeatedly to find a low-boom supersonic transport that also satisfies the specified mission performance requirements [5,6], even when an aeropropulsive CFD simulation is required for sonic boom analysis. The "low-boom" qualifier in this paper means the potential to attain an undertrack sonic boom ground noise level below 70 PLdB at the start of overland cruise (SOC). It is quantified by a close match between the reversed equivalent area ($A_{e,r}$) [7] of the supersonic aircraft and an $A_{e,r}$ target with an undertrack sonic boom ground noise level below 70 PLdB. The sonic boom ground noise limit of 70 PLdB is based on the NASA N+3 low-boom goal [1], which could be replaced by another limit if needed. The specified mission performance requirements include a low-boom overland mission for airport pairs over the continental US and an unrestricted overwater mission for transatlantic commercial flights.

Achieving low-boom ground noise level goal in the undertrack direction at SOC is only the first step in the development of a low-boom supersonic transport. In reality, a low-boom supersonic transport must achieve a low-boom ground noise level goal in all azimuthal directions for the entire mission trajectory. Ueno and Makino [8] developed a robust design method that starts with an $A_{e,r}$ target for each selected off-track direction that reduces the off-track ground noise level. Then they used a conversion and blending process to generate one target for local shape modifications that might lead to an improvement of the low-boom characteristics in five azimuthal directions. Ordaz, Wintzer, and Rallabhandi [9] used two inverse design targets for dp/p at two body lengths away from the aircraft in two azimuthal directions of 0 and 25 deg to demonstrate a robust design method. These dp/p targets were generated using an adjoint-based optimization method [10]. For inverse design optimization at multiple azimuthal angles, one unanswered question is the feasibility of simultaneously matching the specified low-boom inverse design targets in the selected azimuthal directions. If these inverse design targets cannot be theoretically achieved simultaneously by a supersonic aircraft, then only different trades of the inverse design errors are possible between the selected azimuthal directions, no matter what optimization method is used to minimize the inverse design errors for the selected azimuthal directions. If the specified inverse design targets in different azimuthal directions have conflicting shape modification requirements, any optimal solution will result in a significant inverse design error for some azimuthal direction, which might lead to a significantly higher sonic boom ground noise level than the desired goal in that azimuthal direction.

This paper continues to push the state of the art for conceptual low-boom design and initiates a study on an inverse design method that can potentially ensure a simultaneous achievement of a given low-boom ground noise level goal over the primary boom carpet for the entire cruise segment. A new analysis method is proposed for assessment of low-boom characteristics of a low-boom supersonic aircraft at any off-design condition. It can be considered as the first step towards developing a low-boom inverse design method that can refine a low-boom configuration to simultaneously achieve a low-boom goal for a given set of off-design conditions. For each off-design condition, the corresponding $A_{e,r}$ is computed. A multiobjective optimization problem is formulated to compute an $A_{e,r}$ target with the lowest sonic boom ground noise level that can be approximately matched by the $A_{e,r}$ for the off-design condition. The potential application of this analysis method is to predetermine a set of $A_{e,r}$ targets for the specified cruise conditions and azimuthal directions that can be used for a simultaneous reduction of the inverse design errors.

The paper is organized as follows. Section II describes the numerical method used for sonic boom ground signature analysis. A published low-boom supersonic transport concept is reanalyzed with 46 passengers in Sec. III, which will be referred to as the Mach 1.7 46-PAX concept. The method for assessment of low-boom characteristics is introduced in Sec. IV. Section V is for assessment of off-design low-boom characteristics of the Mach 1.7 46-PAX concept. A potentially feasible path for robust low-boom inverse design optimization is briefly discussed in Sec. VI and the conclusions are given in Sec. VII.

II. Sonic Boom Analysis Method

The sonic boom analysis in this paper uses the standard method documented in the Sonic Boom Prediction Workshop III [4,11]: dp/p at three body lengths (3BL) away from the aircraft in a given azimuthal direction is used as the boundary condition of an augmented Burgers equation for propagation through the atmosphere to the ground.

The Euler CFD solver Cart3D [12] is used for all CFD analyses in this paper. An automated meshing process [13] for Cart3D is used to generate a mesh to compute off-body pressures at 3BL away from the aircraft in any azimuthal direction. The azimuthal angle of 0 deg is the undertrack direction (see the top right insert in Fig. 1). For off-body pressure calculation using a Cartesian mesh, the aircraft geometry is first rotated around the pitch axis so that the shocks below the aircraft on the symmetry plane are approximately parallel to the *z*-axis of the Cartesian mesh. Then the aircraft geometry is rotated around the roll axis so that $y = 0$ corresponds to the specified azimuthal direction (see the rotated aircraft geometry inserts in Fig. 1). With engines modeled as flow-through nacelles, this results in a mesh of approximately 30 and 72 million cells for undertrack ($\theta = 0$ deg) and off-track ($\theta > 0$ deg) pressure calculation, respectively, at 3BL away from the aircraft. The smaller mesh size for the undertrack pressure calculation is due to the symmetry of the flow field with respect to $y = 0$, which means that only a mesh in $y \geq 0$ is required for Cart3D analysis. Each mesh has about 275 grid points to define the pressure at 3BL away from the aircraft in the specified azimuthal direction. For visualization of the off-body pressure solution, the Cartesian mesh is rotated around the *y*-axis to realign the flow direction horizontally as shown in Fig. 1, which illustrates an off-body pressure solution at 3BL away from the aircraft for azimuthal angle of 30 deg.

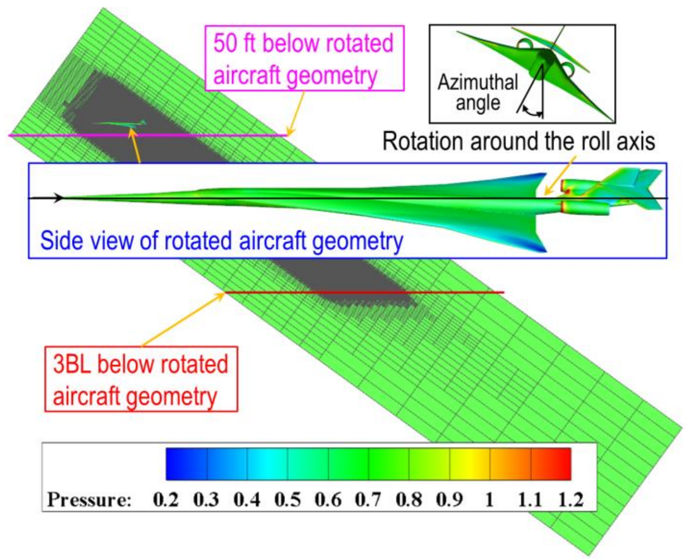

Fig. 1 Rotated view of Cartesian mesh for off-body pressure calculation in azimuthal direction.

The sonic boom ground signature is computed by solving an augmented Burgers equation [14-18] to propagate the off-body pressure at 3BL away from the aircraft in an azimuthal direction to the ground through the standard atmosphere. The humidity profile for the standard atmosphere is based on ANSI S1.26 [19]. The PLdB value [2] of the ground signature is used to measure the sonic boom loudness on the ground in the azimuthal direction at a given cruise condition, which is defined by the cruise Mach, cruise altitude, and angle of attack (AoA) of the aircraft.

An $A_{e,r}$ target is an ideal shape of $A_{e,r}$ for a supersonic configuration to achieve a low sonic boom ground noise level. The calculation of a ground signature of an $A_{e,r}$ target requires an additional step of converting the $A_{e,r}$ target to *dp/p*, which is based on a formula by Whitham that approximates a supersonic configuration by a body of revolution for sonic boom analysis (see Eqs. (14), (69), and (70) in Ref. [20]). The approximation formula for converting any A_e to *dp/p* at 50 ft away from the underlying supersonic configuration represented by A_e is Eq. (6) in Ref. [21], which simplifies Whitham's formula by removing the nonlinear correction term for longitudinal location. The distance of 50 ft is based on the best practices for computing the ground signature of A_e. The numerical formulas for solving Eq. (6) in Ref. [21] are Eqs. (12) and (13) in Ref. [22].

A solver of an augmented Burgers equation, sBOOM 2.8.6 [15], was updated as sBOOM 2.9.0 using a fully conservative and dual-consistent numerical scheme [16]. Due to initial discrepancies of the two versions of sBOOM that were caused by a bug in a prerelease version of sBOOM 2.9.0, we were concerned about the accuracies of our previous low-boom design results in Refs. [5,6] based on sBOOM 2.8.6. So, another solver [17] of the augmented Burgers equation in PCBoom 7.3 [18] was used to verify the accuracy of the computed ground signature. Even though the three solvers use different numerical methods to solve the same augmented Burgers equation, the computed ground signatures from these solvers are nearly identical for every test case we have computed. This provides an indirect assurance that these solvers solve the same augmented Burgers equation consistently. Figure 2 shows the *dp/p* at 90 ft below a supersonic configuration with body length of 90 ft, along with the ground signatures for *dp/p* computed by sBOOM and PCBoom. The cruise altitude is 50,397 ft and the cruise Mach is 1.4. For each solver, the input control parameters are selected to yield a high-resolution solution of the ground signature with negligible differences of the analysis results if the signature resolution is further refined. The ground signatures in Fig. 2 have 40,001 and 32,768 data points from sBOOM and PCBoom, respectively. Because the three solvers generate nearly identical ground signatures with the same PLdB value, we use sBOOM 2.8.6 for sonic boom analysis in this paper.

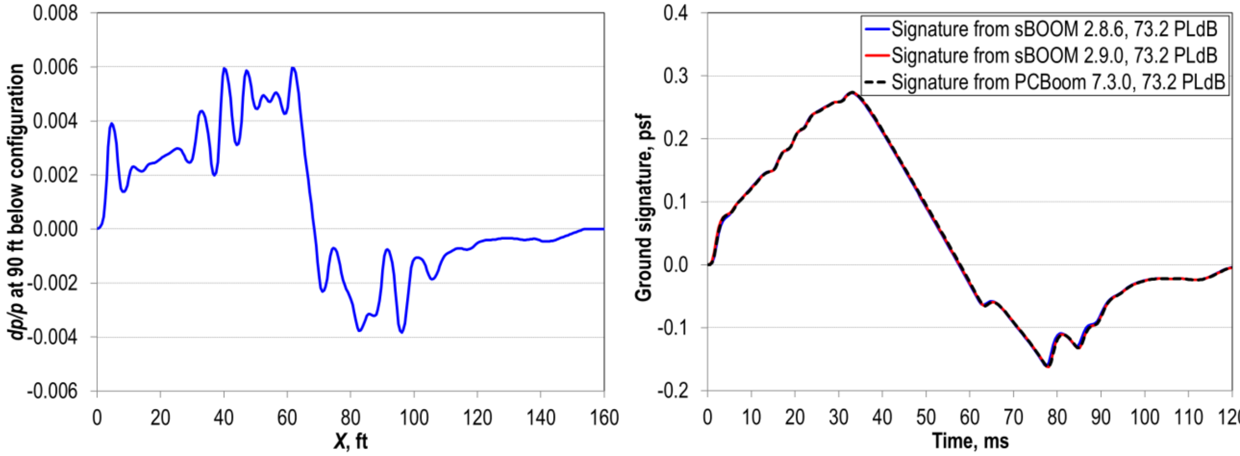

Fig. 2 Comparison of ground signatures generated by three solvers of augmented Burgers equation.

III. Low-Boom Supersonic Concept with Low-Boom Mission Profile

The Mach 1.7 46-PAX concept in Fig. 3 is selected for demonstration of the proposed analysis method for assessment of off-design low-boom characteristics. The Mach 1.7 46-PAX concept is derived from a low-boom concept with 40 passengers, referred to as the Mach 1.7 40-PAX concept [6], which was designed to approximately match an $A_{e,r}$ target of 69.9 PLdB in the undertrack direction at SOC [5]. The Mach 1.7 46-PAX concept has the same OML as the Mach 1.7 40-PAX concept. The low-boom cruise altitude and maximum takeoff gross weight of the Mach 1.7 46-PAX concept are derived iteratively to ensure that i) its AoA at SOC is 2.3 deg (which is the AoA for the Mach 1.7 40-PAX concept at SOC), and ii) its undertrack $A_{e,r}$ matches an $A_{e,r}$ target with an undertrack sonic boom ground noise level below 70 PLdB at SOC (see the PLdB value of the target signature in Fig. 4).

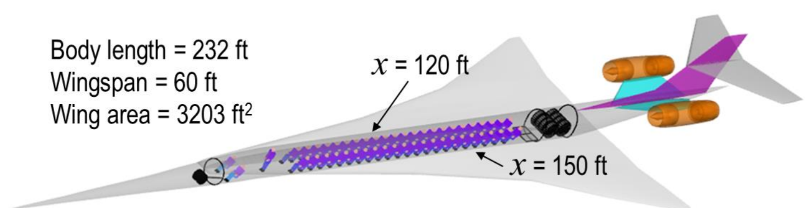

Fig. 3 Mach 1.7 46-PAX low-boom concept.

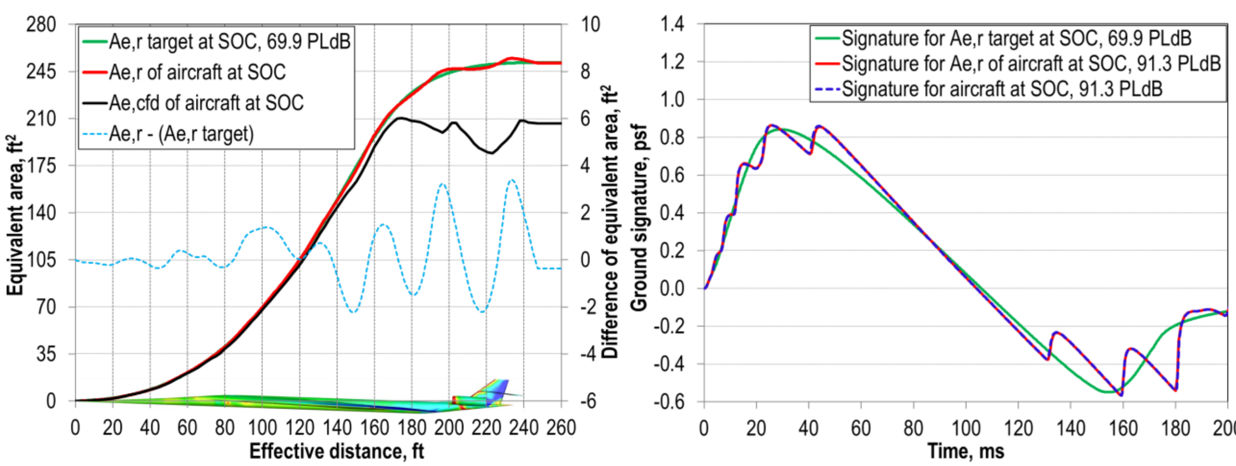

Fig. 4 Equivalent areas and ground signatures of Mach 1.7 46-PAX concept in undertrack direction at SOC.

For any Euler solver and fixed OML with flow-throw nacelles, an aircraft's undertrack *dp/p* at 3BL below the aircraft is invariant with respect to altitude change (see Fig. 5a) as long as the AoA (or lift coefficient) and cruise Mach number are fixed. So, if the undertrack $A_{e,r}$ of a supersonic aircraft is an acceptable inverse design of an $A_{e,r}$ target with ground noise level of 69.9 PLdB, then this aircraft has the same undertrack $A_{e,r}$ at any higher altitude with the same AoA. Moreover, the same $A_{e,r}$ target at the higher cruise altitude also has a ground noise level below 69.9 PLdB. For example, the Mach 1.7 46-PAX concept with AoA of 2.3 deg is also an acceptable inverse design for the same $A_{e,r}$ target in Fig. 4 with undertrack sonic boom ground noise level of 67.4 PLdB at the cruise ceiling of 60,000 ft (see Fig. 5b).

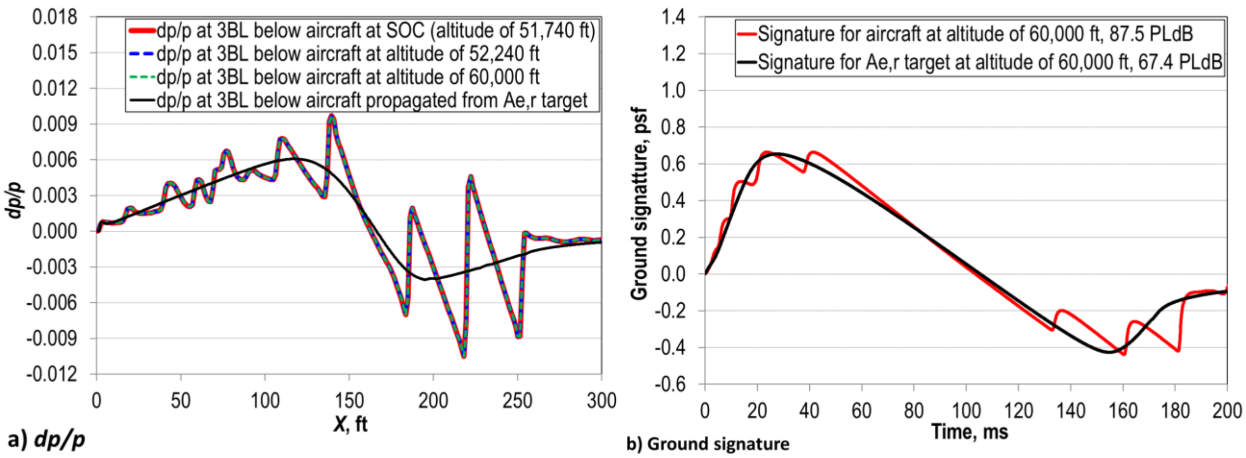

Fig. 5 *dp/p* for various altitudes and undertrack signatures at cruise ceiling when AoA = 2.3 deg.

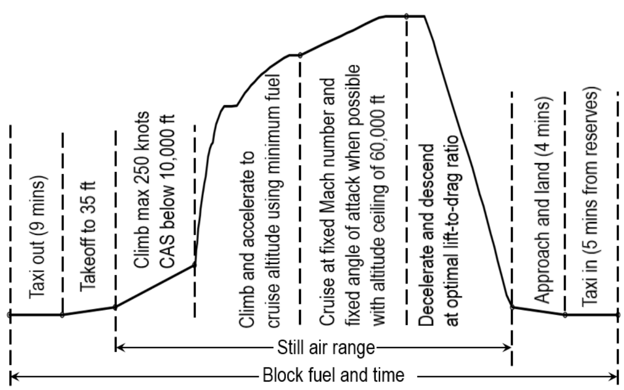

Fig. 6 Low-boom mission profile.

Table 1 Mach 1.7 46-PAX concept

Variable	Value	Variable	Value
Seat pitch, in	38	Low-boom angle of attack, deg	2.30
Max takeoff gross weight, lb	144,760	Altitude at start of overland cruise, ft	51,740
Zero fuel weight, lb	75,683	PLdB of low-boom inverse design target	69.9
Overwater cruise Mach	1.8	Weight at start of cruise, lb	136,643
Overland cruise Mach	1.7	Block fuel for maximum range, lb	64,655
Takeoff field length, ft	8504	Overwater range, nm	3671
Approach velocity, kts	126	Overland range, nm	3725

So, the overland mission profile with a fixed low-boom cruise altitude (see Fig. 5 in Ref. [6]) is replaced by the low-boom mission profile in Fig. 6 for assessment of off-design low-boom characteristics and analysis of the mission performance. This low-boom mission profile allows a low-boom concept to retain the designed low-boom characteristics at SOC as much as possible during the cruise. It also improves the overland cruise performance of a low-boom concept due to the increasing cruise altitude. The weight and performance data of the Mach 1.7 46-PAX concept using the low-boom mission profile in Fig. 6 are listed in Table 1. If the mission profile for overland flight used a fixed cruise altitude of 51,740 ft to analyze the overland performance, then its overland range would be 3314 nm instead of 3725 nm using fixed AoA.

IV. Method for Assessment of Low-Boom Characteristics

In this paper, the low-boom characteristics of a supersonic aircraft is defined by the sonic boom ground noise level of an $A_{e,r}$ target that can be approximately matched by the aircraft's $A_{e,r}$ in an azimuthal direction at a given cruise condition of the low-boom mission profile in Fig. 6. The $A_{e,r}$ of the aircraft for each azimuthal direction is obtained by reversely propagating the off-body pressure at 3BL to 50 ft away from the aircraft (see Fig. 1) using an augmented Burgers equation in the azimuthal direction, converting the reversely propagated pressure to Whitham's F-function, and calculating the corresponding equivalent area of Whitham's F-function. The details for calculating the $A_{e,r}$ in the undertrack direction can be found in Ref. [23]. The same method works for $A_{e,r}$ in any azimuthal direction after rotating the aircraft geometry as shown in Fig. 1. A supersonic aircraft typically has different $A_{e,r}$ shapes for different azimuthal directions.

The assessment of low-boom characteristics of a supersonic aircraft in an azimuthal direction of θ deg is formulated as the following multiobjective optimization problem for simultaneous minimization of the ground noise level of an $A_{e,r}$ target, denoted by $A_e(\theta)$, and the difference between $A_e(\theta)$ and the aircraft's $A_{e,r}$, denoted by $\|A_e(\theta) - A_{e,r}(\theta)\|$.

$$\min_{\boldsymbol{d}} \{\text{PLdB}[A_e(\theta)], \|A_e(\theta) - A_{e,r}(\theta)\|\} \tag{1}$$

The notation PLdB[$A_e(\theta)$] represents the PLdB value of the ground signature of $A_e(\theta)$ in the azimuthal direction of θ deg. The $A_e(\theta)$ in Eq. (1) is parameterized by the control points of a Bezier curve. For $0 \le t \le 1$, the corresponding point (x, $A_e(x,\theta)$) on a Bezier curve is defined as follows.

$$\begin{aligned} x(t) &= l_e \cdot t^9 + \sum_{j=1}^{8} x_{c,j} \cdot \frac{9!}{j!\,(9-j)!} \cdot t^j \cdot (1-t)^{9-j} \\ A_e(x(t),\theta) &= y_{c,8} \cdot t^9 + \sum_{j=2}^{8} y_{c,j} \cdot \frac{9!}{j!\,(9-j)!} \cdot t^j \cdot (1-t)^{9-j} \end{aligned} \tag{2}$$

In this paper, a Bezier curve with 10 control points is used as a parametric form of $A_e(\theta)$. In Refs. [5,6,23], the parametric form of an $A_{e,r}$ target has only 8 control points. However, the George-Seebass-Darden low-boom inverse design theory [21,24] implicitly depends on the validity of the inverse relation between an equivalent area and an F-function (see Theorems 1 and 2 in Ref. [22]). This inverse relation is valid if and only if the slope of the equivalent area is zero at $x_e = 0$ and $x_e = l_e$ (see Remark 2 after Theorem 1 in Ref. [22]). So, theoretically, the slope of an $A_{e,r}$ target must be zero at $x_e = 0$ and $x_e = l_e$, even though minor deviations of the slope at $x_e = 0$ and $x_e = l_e$ from zero could be considered as acceptable numerical errors for low-boom inverse design of $A_{e,r}$. To be consistent with the theory in Ref. [22], two additional control points are added to enforce the zero-slope constraints at $x_e = 0$ and $x_e = l_e$. The parametric form of $A_e(\theta)$ in Eq. (2) always satisfies the zero-slope constraint at $x_e = 0$ and $x_e = l_e$. To keep the number of design variables for an $A_{e,r}$ target the same as before, $x_{c,1}$ and $x_{c,8}$ are fixed with $x_{c,1} = 0.001 \cdot l_e$ and $x_{c,8} = 0.999 \cdot l_e$ in this paper. So, the design vector $\boldsymbol{d}$ in Eq. (1) has $x_{c,j}$ ($2 \le j \le 7$) and $y_{c,j}$ ($2 \le j \le 8$) as the components with a total of 13 design variables. The choices for the resulting parametric form of an $A_{e,r}$ target are empirical. But this parametric form is adequate for the applications in this paper. That is, every $A_{e,r}(\theta)$ in this paper can be fitted by an $A_e(\theta)$ with $\|A_e(\theta) - A_{e,r}(\theta)\| \le \epsilon$. If this parametric form were not flexible enough for $A_{e,r}$ targets, $x_{c,1}$ and $x_{c,8}$ would also be used as design variables in Eq. (1). If needed, more control points could be used to define an $A_{e,r}$ target in Eq. (1). But more design variables will require more time to solve Eq. (1).

The selected optimal solution of Eq. (1) as the $A_{e,r}$ target of $A_{e,r}(\theta)$ is the Pareto optimal solution with the minimum value of PLdB[$A_e(\theta)$] while the inverse design error of $A_{e,r}(\theta)$ for the selected $A_{e,r}$ target is within the error tolerance, i.e., $\|A_e(\theta) - A_{e,r}(\theta)\| \le \epsilon$. For easy reference, this Pareto optimal solution will be denoted by $A_{e,r}^{\text{target}}(\theta)$. In this paper, the acceptable error tolerance ϵ is $0.007 \cdot A_{e,r}(l_e,\theta)$, which was used in Refs. [5,6]. If $A_{e,r}(\theta)$ is an acceptable inverse design for $A_{e,r}^{\text{target}}(\theta)$, then the underlying configuration has the potential to achieve a ground noise level of PLdB[$A_{e,r}^{\text{target}}(\theta)$] at the specified cruise condition and azimuthal direction. Otherwise, the underlying configuration without any shape modification is not considered to have any quantifiable low-boom characteristics at the specified cruise condition and azimuthal angle. In this case, a more flexible parametric model of $A_e(\theta)$ is required for assessment of off-design low-boom characteristics of the underlying supersonic configuration for the required inverse design error constraint.

To gain an intuitive understanding of $\|A_{e,r}^{target}(\theta) - A_{e,r}(\theta)\|$ in terms of shape modifications for a low-boom inverse design, we need the following approximation relation between $A_{e,r}$ and $A_{e,CFD}$.

$$A_{e,r}(x_e, \boldsymbol{D}) - A_{e,r}(x_e, \boldsymbol{D}_0) \approx A_{e,CFD}(x_e, \boldsymbol{D}) - A_{e,CFD}(x_e, \boldsymbol{D}_0) \quad \text{for } 0 \le x_e \le l_e \tag{3}$$

Equation (3) was first formulated and verified in Ref. [25] for the undertrack direction. But it is also true for an off-track direction, which is the undertrack direction for a rotated aircraft geometry (see Fig. 1). For simplicity, we omit the azimuthal angle θ in Eq. (3). Note that $A_{e,CFD}$ [20,26] is the sum of the equivalent area due to lift and the equivalent area due to volume for the rotated aircraft geometry. So, the values of $A_{e,CFD}$ around a location of x_e can be increased/decreased by increasing/decreasing the lift and volume distributions of the rotated aircraft geometry around the same location of x_e. By Eq. (3), this corresponds to increasing/decreasing the $A_{e,r}$ values around the same location of x_e. Now, assume that $\boldsymbol{D}$ is indeed the inverse design whose $A_{e,r}(\boldsymbol{D})$ matches $A_{e,r}^{target}(\theta)$ for $A_{e,r}(\theta) = A_{e,r}(\boldsymbol{D}_0)$, the reversed equivalent area of a baseline design $\boldsymbol{D}_0$. Then Eq. (3) implies the following approximation formula, which indicates that the inverse design error $\|A_{e,r}^{target}(\theta) - A_{e,r}(\boldsymbol{D}_0)\|$ for the baseline design $\boldsymbol{D}_0$ does approximately represent the amount of the required lift and volume modifications of $\boldsymbol{D}_0$ to match the $A_{e,r}$ target.

$$\|A_{e,r}^{target}(\theta) - A_{e,r}(\boldsymbol{D}_0)\| \approx \|A_{e,CFD}(\boldsymbol{D}) - A_{e,CFD}(\boldsymbol{D}_0)\| \tag{4}$$

Equation (1) is solved using the non-dominated sorting genetic algorithm II (NSGA II) in ModelCenter [27]. NSGA II requires finite lower and upper bounds for the design variables. The target $A_{e,r}^{target}(\theta)$ could be obtained by solving Eq. (1) with a set of bound constraints on $\boldsymbol{d}$: $0 \le x_{c,j} \le l_e$ and $0 \le y_{c,j} \le 1.5 \cdot A_{e,r}(l_e, \theta)$. In practice, more restrictive bounds of $\boldsymbol{d}$ are used empirically to reduce the size of the design space in search of $A_{e,r}^{target}(\theta)$.

The computing equipment for solving Eq. (1) is two Windows servers with 40 cores of Intel Xeon CPUs at 2.4 GHz, with ModelCenter running on one server and the analysis codes running on another. The optimization run uses ModelCenter's parallel computing capability to perform 16 design analyses simultaneously. It takes about 12 hours to generate approximately 5,000 designs. While the wall-clock time for solving Eq. (1) depends on $A_{e,r}(\theta)$ and the loads on the Windows servers, as well as the accuracy requirement for the Pareto frontier, $A_{e,r}^{target}(\theta)$ is typically obtained within 5 days for all the analysis cases in this paper, using multiple optimization runs with various bounds of $\boldsymbol{d}$.

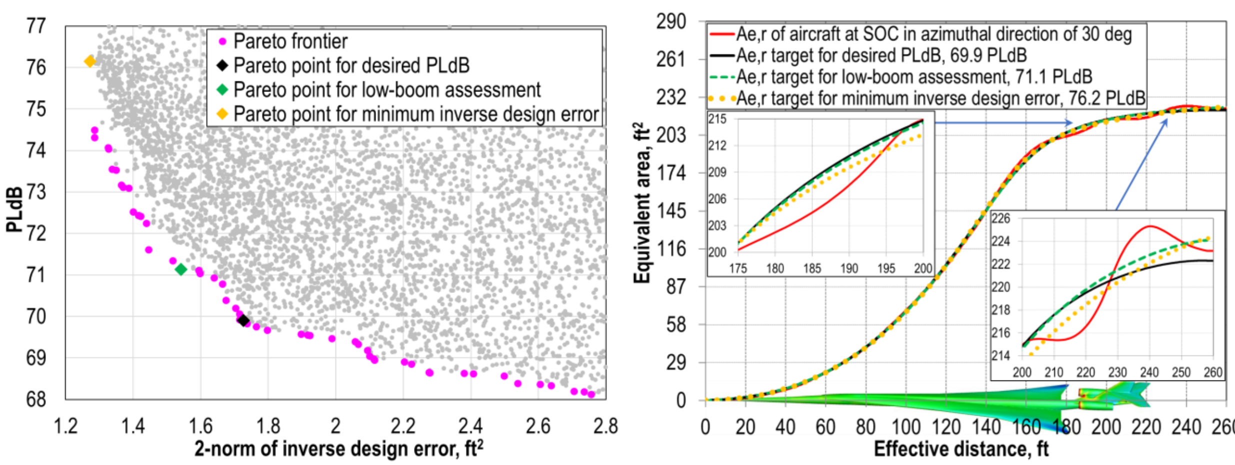

Fig. 7 Selected $A_{e,r}$ targets from Pareto frontier for Eq. (1) with appropriate bounds of $\boldsymbol{d}$.

The analysis method of computing $A_{e,r}^{target}(\theta)$ is applied to the Mach 1.7 46-PAX concept at SOC with an azimuthal angle of 30 deg as an example. In this case, $A_{e,r}(l_e, \theta)$ of the aircraft is 223.2 ft², l_e = 258.1 ft, and ϵ = 1.56 ft². Here, l_e is determined by the undertrack Mach angle cut plane for the rotated aircraft geometry in Fig. 1. The Pareto frontier in Fig. 7 is generated using a design space of $\boldsymbol{d}$ defined by a range of $0.2 \cdot l_e$ for $x_{c,j}$ and a range of $0.4 \cdot A_{e,r}(l_e, \theta)$ for $y_{c,j}$. The design space is centered around a design vector satisfying $\|A_e(\theta) - A_{e,r}(\theta)\| \le \epsilon$. The reason to find a solution of

$\|A_e(\theta) - A_{e,r}(\theta)\| \le \epsilon$ first is to ensure that the parametric form of $A_e(\theta)$ is flexible enough to fit $A_{e,r}(\theta)$ accurately. The Pareto frontier in Fig. 7 is derived from about 18,000 designs generated by NSGA II within a wall-clock time of 46 hours. Three targets are plotted in Fig. 7 to show trades between the PLdB value and inverse design error. These $A_{e,r}$ targets have approximately identical shapes but noticeably different PLdB values. This shows a high sensitivity of the PLdB value of the ground signature with respect to the shape of $A_{e,r}$ target.

The Mach 1.7 46-PAX concept is an acceptable inverse design of $A_{e,r}^{\text{target}}(\theta)$ that has a sonic boom ground noise level of 71.1 PLdB in azimuthal direction of 30 deg. Such an analysis method provides a quantitative assessment of low-boom characteristics of a supersonic configuration at different cruise conditions and azimuthal directions. Note that, once the Mach 1.7 46-PAX concept is refined for minimization of the sonic boom ground noise level in a preliminary design phase, an off-design assessment of low-boom characteristics could be easily determined by the PLdB value of the ground signature of the refined configuration at the given off-design condition. So, this assessment method of low-boom characteristics is specifically developed for conceptual design of low-boom supersonic aircraft.

V. Assessment of Low-Boom Characteristics of Mach 1.7 46-PAX Concept

The inverse design optimization for the Mach 1.7 46-PAX concept at SOC starts with an $A_{e,r}$ target with undertrack sonic boom ground noise level below 70 PLdB and matches the undertrack $A_{e,r}$ of the aircraft with the $A_{e,r}$ target within the tolerance ϵ (see the inverse design error curve Fig. 4). The analysis method in Sec. IV will be applied to assess off-design low-boom characteristics of the Mach 1.7 46-PAX concept. An off-design condition for the Mach 1.7 46-PAX concept is defined by either a cruise condition not at SOC or a nonzero azimuthal direction for sonic boom analysis. A representative set of off-design conditions will be used to give an overall assessment on whether the Mach 1.7 46-PAX concept has any significant deficiency in low-boom characteristics over the primary boom carpet for the entire cruise segment. Low-boom characteristics at a non-cruise condition is also important but they are not discussed in this paper because different sonic boom analysis methods are required for non-cruise conditions.

First, consider the low-boom characteristics in the undertrack direction for the entire cruise segment. Note that *dp/p* at 3BL away from the aircraft with a fixed AoA is identical at any cruise condition in a fixed azimuthal direction. As a result, the Mach 1.7 46-PAX concept is an acceptable low-boom inverse design for the same undertrack $A_{e,r}$ target at any cruise condition before it changes the AoA after reaching the cruise ceiling in the low-boom mission profile. For the same *dp/p*, the corresponding ground signature has a lower noise level if the cruise altitude is higher, which is based on our numerical verifications of a variety of *dp/p* shapes. An intuitive interpretation is that the loudness of sonic boom generated by a fixed waveform decreases as the propagation distance increases. So, the ground noise level of the same $A_{e,r}$ target decreases when the cruise altitude increases (see Figs. 4 and 5).

After reaching the cruise ceiling of 60,000 ft, the Mach 1.7 46-PAX concept must reduce the AoA to match the reduced cruise weight as the fuel is consumed during the cruise. At the end of cruise, the undertrack $A_{e,r}$ of the Mach 1.7 46-PAX concept is very different from the $A_{e,r}$ target at SOC as expected. However, the analysis method in Sec. IV shows that the Mach 1.7 46-PAX concept is also an acceptable inverse design for an undertrack $A_{e,r}$ target with sonic boom ground noise level of 66.0 PLdB (see Fig. 8). This shows that the Mach 1.7 46-PAX concept has low-boom $A_{e,r}$ shapes in the undertrack direction with the potential of achieving sonic boom ground noise levels below 70 PLdB for the entire cruise segment.

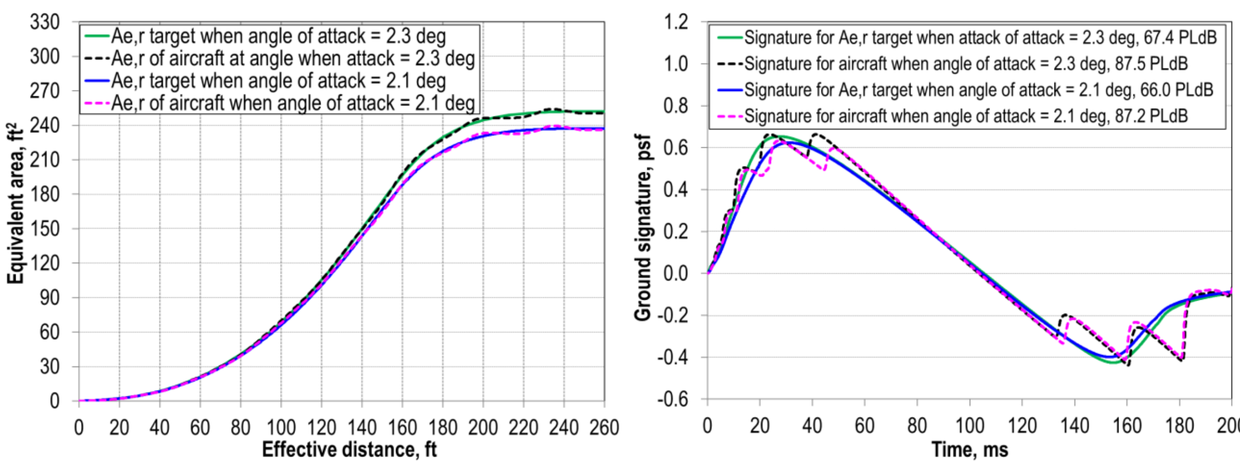

Fig. 8 A_e **distributions and signatures for aircraft cruising at 60,000 ft in undertrack direction.**

For low-boom characteristics in off-track directions, four off-track angles are used to show the off-track low-boom characteristics of the Mach 1.7 46-PAX concept at SOC. The analysis method in Sec. IV is used to compute $A_{\mathrm{e,r}}^{\mathrm{target}}(\theta)$ for $A_{\mathrm{e,r}}(\theta)$ of the Mach 1.7 46-PAX concept at SOC with θ = 25, 30, 35, and 40 deg. Each $A_{\mathrm{e,r}}(\theta)$ is an acceptable inverse design for the $A_{\mathrm{e,r}}$ target of $A_{\mathrm{e,r}}^{\mathrm{target}}(\theta)$ with inverse design error $\left\|A_{\mathrm{e,r}}^{\mathrm{target}}(\theta) - A_{\mathrm{e,r}}(\theta)\right\| \leq \epsilon$. The $A_{\mathrm{e,r}}(\theta)$ shapes are approximately identical for $x_{\mathrm{e}} < 120$ ft (see the A_{e} shapes in Fig. 9), so the configuration does behave like a body of revolution at SOC for $x_{\mathrm{e}} < 120$ ft. A small portion of the wing is within the range of $x_{\mathrm{e}} < 120$ ft (see Fig. 3) and the fuselage shape is not symmetric with respect to the roll axis of the aircraft at SOC. This indirectly confirms that Whitham-Walkden's body-of-revolution approximation [20,28] of a supersonic configuration for sonic boom analysis is accurate for a wing-body configuration if the lift force is weak, which is consistent with the assumption of a wing at a small incidence to the stream in Refs. [20,28]. Note that $A_{\mathrm{e,CFD}}$ and $A_{\mathrm{e,r}}$ in the undertrack direction at SOC are approximately identical for $x_{\mathrm{e}} < 120$ ft (see the A_{e} shapes in Fig. 4), which indicates that $A_{\mathrm{e,r}}$ is an aft correction of $A_{\mathrm{e,CFD}}$ for sonic boom analysis of any supersonic aircraft using a body-of-revolution approximation. The nearly identical ground signatures for *dp/p* at 3BL and $A_{\mathrm{e,r}}$ (see the ground signatures in Fig. 4) show that $A_{\mathrm{e,r}}$ represents an accurate body-of-revolution approximation of the supersonic aircraft for sonic boom analysis.

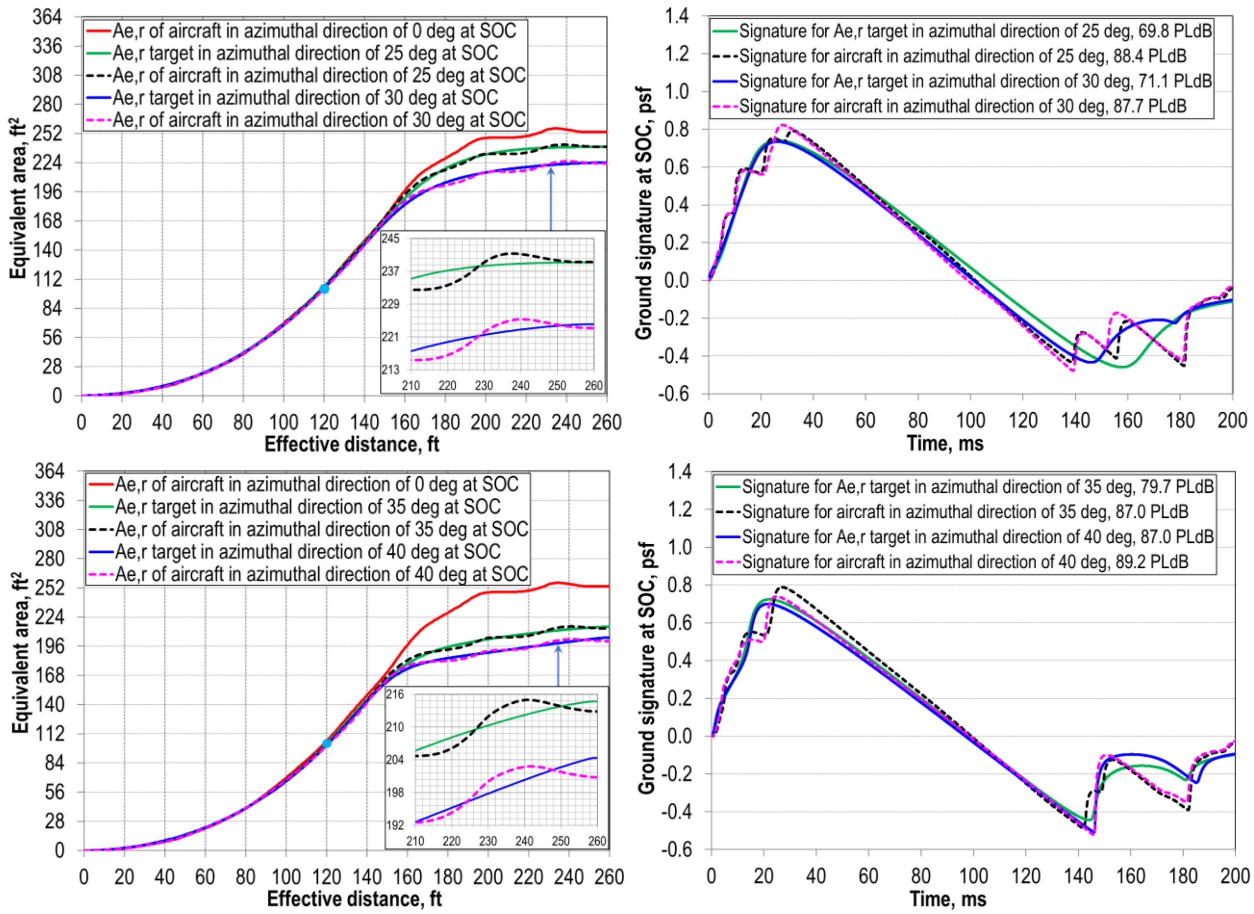

Fig. 9 Equivalent areas and ground signatures in different azimuthal directions at SOC.

As θ increases from 0 to 25 deg, the aft shape of $A_{\mathrm{e,r}}(\theta)$ gradually bends downward proportionally starting at about $x_{\mathrm{e}} = 150$ ft (see the A_{e} shapes for θ = 0 and 25 deg in Fig. 9). This allows the aft shape of $A_{\mathrm{e,r}}^{\mathrm{target}}(\theta)$ to bend in a similar way to match $A_{\mathrm{e,r}}(\theta)$ while maintaining the ground noise level below 70 PLdB for $A_{\mathrm{e,r}}^{\mathrm{target}}(\theta)$. For θ = 30 deg, the aft shape of $A_{\mathrm{e,r}}(\theta)$ still bends downward proportionally starting at about $x_{\mathrm{e}} = 150$ ft, but the best aft fit of $A_{\mathrm{e,r}}(\theta)$ requires a slightly positive slope near the end of effective range, which conflicts with the zero slope constraint at $x_{\mathrm{e}} = l_{\mathrm{e}}$. Even though $A_{\mathrm{e,r}}^{\mathrm{target}}(\theta)$ has an analytical zero slope at $x_{\mathrm{e}} = l_{\mathrm{e}}$, the forced change of $A_{\mathrm{e,r}}^{\mathrm{target}}(\theta)$ from a slightly positive slope to the zero slope near $x_{\mathrm{e}} = l_{\mathrm{e}}$ is manifested by a small kink in the ground signature of $A_{\mathrm{e,r}}^{\mathrm{target}}(\theta)$ around 180 ms (see the target signature for θ = 30 deg in Fig. 9). The ground noise level of $A_{\mathrm{e,r}}^{\mathrm{target}}(\theta)$ is 71.1 PLdB, slightly higher than those for azimuthal directions of 0 and 25 deg. For θ = 35 and 40 deg, $A_{\mathrm{e,r}}^{\mathrm{target}}(\theta)$ requires an approximately linear fit with a positive slope for $x_e \geq 210$ ft. The corresponding $A_{e,r}$ targets have ground noise levels of 79.7 and 87.0 PLdB, respectively. The shapes of the target and actual ground signatures are quite similar for each azimuthal direction, which is another indirect confirmation of the validity of inverse design optimization using $A_{e,r}$. The PLdB value of $A_{e,r}^{target}(\theta)$ provides a quantitative assessment on degradation of the undertrack low-boom $A_{e,r}$ shape in the azimuthal direction in conceptual low-boom design phase.

VI. Potential Application to Robust Low-Boom Inverse Design

The analysis method in Sec. III can be considered as the sonic boom analysis of low-boom characteristics of a supersonic concept over the primary boom carpet for the entire cruise segment. However, this analysis method can be slightly modified for finding a compatible set of $A_{e,r}$ target for a given set of cruise conditions and azimuthal directions. Here a set of compatible $A_{e,r}$ targets means that the inverse design errors with respect to this set of $A_{e,r}$ targets can be simultaneously reduced within a given tolerance using modifications of the aircraft's OML.

Now, let $A_{e,r}(\theta)$ be the reversed equivalent area of a supersonic configuration corresponding to a pair of cruise condition and azimuthal direction of θ deg. Assume that there exists an appropriate Pareto optimal solution $A_{e,pareto}(\theta)$ of Eq. (1) such that all the inverse design error functions, $A_{e,pareto}(\theta) - A_{e,r}(\theta)$, have the positive sign over a specified range of x_e. By Eq. (3), if the physical volume of this supersonic configuration is increased in the specified range of x_e, then the values of $A_{e,r}(\theta)$ over the specified range of x_e will increase, which will lead to a simultaneous reduction of the inverse design errors for the specified pairs of cruise conditions and azimuthal angles. Equation (1) provides a tradeoff between an easy-to-match target and the ground noise level of the target for low-boom inverse design optimization for any pair of cruise condition and azimuthal direction. Moreover, Eq. (1) generates a variety of $A_{e,r}$ targets for each pair of cruise condition and azimuthal direction (see Fig. 7). In this paper, one of those targets is used to assess the low-boom characteristics of the underlying supersonic concept at an off-design condition. Future research will be focused on how to use these targets to determine a set of compatible $A_{e,r}$ targets for robust inverse design optimization over the primary boom carpet for the entire cruise segment.

VII. Conclusions

An analysis method for assessment of low-boom characteristics of a supersonic concept is proposed in this paper. It aims to provide a quantitative method to assess the low-boom characteristics of a given supersonic concept at any cruise condition and azimuthal direction. This analysis method finds an $A_{e,r}$ target that has the lowest sonic boom ground noise level and can be approximately matched by the $A_{e,r}$ of the supersonic concept for the specified cruise condition and azimuthal direction. A low-boom mission profile is defined for any supersonic concept designed for low boom at SOC. This low-boom mission not only allows a supersonic concept to retain the designed low-boom characteristics at SOC as much as possible for the entire cruise segment, but also improves the overland cruise efficiency of the supersonic concept.

The analysis method is applied to assess the off-design low-boom characteristics of the Mach 1.7 46-PAX concept, which was designed for a low-boom $A_{e,r}$ shape at SOC in the undertrack direction. It shows that the Mach 1.7 46-PAX concept is an acceptable low-boom inverse design for an $A_{e,r}$ target with ground noise level below 70 PLdB in the undertrack direction at any cruise condition. The Mach 1.7 46-PAX concept also has a low-boom $A_{e,r}$ shape at SOC for any off-track direction with azimuthal angle no more than 25 deg, while the low-boom $A_{e,r}$ shape matches an $A_{e,r}$ target with sonic boom ground noise level less than 70 PLdB. However, as the azimuthal angle increases from 25 to 40 deg, the Mach 1.7 46-PAX concept starts to lose the low-boom characteristics designed for the undertrack direction at SOC. In particular, the $A_{e,r}$ of the Mach 1.7 46-PAX concept in the off-track angle of 40 deg can only be considered as an acceptable inverse design of an $A_{e,r}$ target with sonic boom ground noise level of 83.1 PLdB.

This paper is the first step of finding a low-boom inverse design method to reduce the sonic boom ground noise level over the primary boom carpet for the entire cruise segment. The ultimate goal is to generate a set of compatible $A_{e,r}$ targets for inverse design optimization at specified pairs of cruise conditions and azimuthal directions.

Acknowledgments

This work is funded by the NASA Commercial Supersonic Technology Project. The authors are grateful to Joel Lonzaga for providing the template files and instructions to run PCBoom 7 for propagation of *dp/p* to the ground.

References

[1] Morgenstern, J., Norstrud, N., Stelmack, M., and Jha, P., "Advanced Concept Studies for Supersonic Commercial Transports Entering Service in 2030-2035 (N+3)," AIAA Paper 2010-5114, June 2010. doi:10.2514/6.2010-5114

[2] Stevens, S., “Perceived Level of Noise by Mark VII and Decibels (E),” *Journal of the Acoustical Society of America*, Vol. 51, No. 2B, 1972, pp. 575–601. doi:10.1121/1.1912880

[3] Chapman, K., “The X Factor—QueSST Exclusive,” *Air International*, IPC Media Limited, London, U. K., Sep. 2022, pp. 28–39, http://www.ipcmedia.com/.

[4] Park, M., and Carter, M., “Low-Boom Demonstrator Near-Field Summary for the Third AIAA Sonic Boom Prediction Workshop,” *Journal of Aircraft*, Vol. 59, No. 3, 2022, pp. 563–577. doi:10.2514/1.C036323

[5] Li, W., and Geiselhart, K., “Multi-objective, Multidisciplinary Optimization of Low-Boom Supersonic Transports Using Multifidelity Models,” *Journal of Aircraft*, Vol. 59, No. 5, 2022, pp. 1137–1151. doi:10.2514/1.C036656.

[6] Li, W., and Geiselhart, K., “Propulsion-Airframe Integration for Conceptual Redesign of a Low-Boom Supersonic Transport,” *Journal of Aircraft*, (2023), accessed Sep. 9, 2023. doi:10.2514/1.C037310

[7] Li, W., and Rallabhandi, S., “Inverse Design of Low-Boom Supersonic Concepts Using Reversed Equivalent-Area Targets,” *Journal of Aircraft*, Vol. 51, No. 1, 2014, pp. 29–36. doi:10.2514/1.C031551

[8] Ueno, A., and Makino, Y., “Robust Low-Boom Design in Primary Boom Carpet,” AIAA Paper 2021-1270, Jan. 2021. doi:10.2514/6.2021-1270

[9] Ordaz, I., Wintzer, M., and Rallabhandi, S., “Full-Carpet Design of a Low-Boom Demonstrator Concept,” AIAA Paper 2015-2261, June 2015. doi:10.2514/6.2015-2261

[10] Rallabhandi, S., “Application of Adjoint Methodology in Various Aspects of Sonic Boom Design,” AIAA Paper 2014-2271, June 2014. doi:10.2514/6.2014-2271

[11] Rallabhandi, S., and Loubeau, A., “Summary of Propagation Cases of the Third AIAA Sonic Boom Prediction Workshop,” *Journal of Aircraft*, Vol. 59, No. 3, 2022, pp. 578–594. doi:10.2514/1.C036327

[12] *Cart3D, Version 1.5*, NASA, URL:https://www.nas.nasa.gov/software/cart3d.html [retrieved 2 Sep. 2023].

[13] Ordaz, I., and Li, W., “Integration of Off-Track Sonic Boom Analysis in Conceptual Design of Supersonic Aircraft,” *Journal of Aircraft*, Vol. 51, No. 1, 2014, pp. 23–28. doi:10.2514/1.C031511

[14] Cleveland, R., Chambers, J., Bass, H., Raspet, R., Blackstock, D., and Hamilton, M., “Comparison of Computer Codes for the Propagation of Sonic Boom Waveforms Through Isothermal Atmospheres,” *Journal of the Acoustical Society of America*, Vol. 100, No. 5, 1996, pp. 3017–3027. doi:10.1121/1.417113

[15] Rallabhandi, S., “Advanced Sonic Boom Prediction Using Augmented Burgers Equation,” *Journal of Aircraft*, Vol. 48, No. 4, 2011, pp. 1245–1253. doi:10.2514/1.C031248

[16] Rallabhandi, S., Nemec, M., and Aftosmis, M., 2023. “Recent Enhancements to Modeling Sonic Boom Propagation using Augmented Burgers' Equation,” AIAA Paper 2023-3727, June 2023. doi:10.2514/6.2023-3727

[17] Lonzaga, J., “Recent Enhancements to NASA’s PCBoom Sonic Boom Propagation Code,” AIAA Paper 2019-3386, June 2019. doi:10.2514/6.2019-3386

[18] Lonzaga, J., Page, J., Downs, R., Kaye, S., Shumway, M., Loubeau, A., and Doebler, W., “PCBoom Version 7 Technical Reference,” NASA/TM-20220007177, Dec. 2022.

[19] Method for Calculation of the Absorption of Sound by the Atmosphere, Annex C, American National Standards Inst., Standard S1.26-1995, New York, 1995.

[20] Whitham, G., “On the Propagation of Weak Shock Waves,” *Journal of Fluid Mechanics*, Vol. 1, No. 3, 1956, pp. 290–318. doi:10.1017/S0022112056000172

[21] Seebass, R., and George, A., “Sonic Boom Minimization,” *Journal of the Acoustical Society of America*, Vol. 51, No. 2C, 1972, pp. 686–694. doi:10.1121/1.1912902

[22] Li, W., “A Theoretical and Computational Revisit of Conversions Between Whitham’s F-Function and Equivalent Area,” NASA/TM-20230002114, May 2023.

[23] Li, W., “Equivalent Area Targets for Inverse Design Optimization with Changing Low-Boom Cruise Conditions,” *AIAA Journal*, Vol. 61, No. 3, 2023, pp. 1260–1269. doi:10.2514/1.J062324

[24] Darden, C., “Minimization of Sonic-Boom Parameters in Real and Isothermal Atmospheres,” NASA TN D-7842, March 1975.

[25] Ordaz, I., and Li, W., “Approximation of Off-Body Sonic-Boom Analysis for Low-Boom Conceptual Design,” *Journal of Aircraft*, Vol. 53, No. 1, 2016, pp. 14–19. doi:10.2514/1.C033159

[26] Seebass, R., “Sonic Boom Theory,” *Journal of Aircraft*, Vol. 6, No. 3, 1969, pp. 177–184. doi:10.2514/3.44032

[27] *ModelCenter, Version 12.0*, Phoenix Integration Inc., URL:http://www.phoenix-int.com [retrieved 26 Oct. 2023].

[28] Walkden, F., “The Shock Pattern of a Wing-Body Combination, Far from the Flight Path,” *Aeronautical Quarterly*, Vol. 9, No. 2, 1958, pp. 164–194. doi:10.1017/S0001925900001372